

Patched and Costal-2 mutations lead to differences in tissue overgrowth autonomy

Shannon L. Moore^a, Frank C. Adamini^a, Erik S. Coopes^a, Dustin Godoy^b, Shyra J. Northington^{a,c}, Jordan M. Stewart^a, Richard L. Tillet^d, Kayla L. Bieser^b, and Jacob D. Kagey^a

^aBiology Department, University of Detroit Mercy, Detroit, Michigan, USA; ^bDepartment of Physical and Life Sciences, Nevada State College, Henderson, Nevada, USA; ^cReBUILDetroit, University of Detroit Mercy, Detroit, Michigan, USA; ^dNevada Institute of Personalized Medicine, University of Nevada, Las Vegas, Nevada, USA

ABSTRACT

Genetic screens are used in *Drosophila melanogaster* to identify genes key in the regulation of organismal development and growth. These screens have defined signalling pathways necessary for tissue and organismal development, which are evolutionarily conserved across species, including *Drosophila*. Here, we have used an FLP/FRT mosaic system to screen for conditional regulators of cell growth and cell division in the *Drosophila* eye. The conditional nature of this screen utilizes a block in the apoptotic pathway to prohibit the mosaic mutant cells from dying via apoptosis. From this screen, we identified two different mutants that mapped to the Hedgehog signalling pathway. Previously, we described a novel *Ptc* mutation and here we add to the understanding of disrupting the Hh pathway with a novel allele of *Cos2*. Both of these Hh components are negative regulators of the pathway, yet they depict mutant differences in the type of overgrowth created. *Ptc* mutations lead to overgrowth consisting of almost entirely wild-type tissue (non-autonomous overgrowth), while the *Cos2* mutation results in tissue that is overgrown in both the mutant and wild-type clones (both autonomous and non-autonomous). These differences in tissue overgrowth are consistent in the *Drosophila* eye and wing. The observed difference is correlated with different deregulation patterns of pMad, the downstream effector of DPP signalling. This finding provides insight into pathway-specific differences that help to better understand intricacies of developmental processes and human diseases that result from deregulated Hedgehog signalling, such as basal cell carcinoma.

ARTICLE HISTORY

Received 22 June 2021
Revised 31 March 2022
Accepted 2 April 2022

KEYWORDS

genetic screen; apoptosis;
cell growth; Hedgehog
signaling

Introduction

Drosophila melanogaster is a long-established model system with particular usefulness in understanding the genetic mechanisms underlying many life processes, including the genetic regulation of growth and development. A large proportion of the genes that regulate growth in developing tissues across species, including humans, were first identified using genetic screens in *Drosophila* [1]. The FLP/FRT genetic system has been used in genetic screens to identify genes involved in regulating growth and differentiation by analysing the ratios of mutant to wild-type tissue and overall ommatidial patterning within the *Drosophila* eye. Genes identified in these screens have been implicated in human diseases, many of which were

initially discovered in *Drosophila* and later found to be disease causing in human [2–5].

In developing our genetic screen, we hypothesized that a subset of mutations would lead to the removal of mutant cells through apoptosis (when homozygous), thus causing specific mutations to be missed in the initial iterations of the FLP/FRT screen [1,6]. Since the inhibition of apoptosis remains a key step during carcinogenesis for cancer cells to avoid a primary defence mechanism [7], this inhibition remains an important genetic process to understand. Therefore, we conducted a second-generation conditional FLP/FRT EMS screen on chromosome 2R in a genetic background blocking apoptosis to identify conditional regulators of cell growth and division [8].

CONTACT Jacob D. Kagey  kageyja@udmercy.edu  Biology Department, University of Detroit Mercy, Detroit, Michigan 48221, USA

 Supplemental data for this article can be accessed [here](#)

© 2022 The Author(s). Published by Informa UK Limited, trading as Taylor & Francis Group.

This is an Open Access article distributed under the terms of the Creative Commons Attribution License (<http://creativecommons.org/licenses/by/4.0/>), which permits unrestricted use, distribution, and reproduction in any medium, provided the original work is properly cited.

A number of growth mutants are conditional with a block in apoptosis (i.e. *scribbled*) providing further rationale for the screen [9].

From this screen, we have previously reported on several conditional regulators of cell growth and cell division including *CPA* and *Shn*, demonstrating the occurrence of these conditional growth mutants [10,11]. Here, we describe the overgrowth caused by two of these mutants identified in the screen that are both part of the Hedgehog signalling pathway, *Patched* (*Ptc*) and *Costal-2* (*Cos2*).

The Hedgehog pathway (Hh) is a highly conserved signalling pathway essential to organismal development [12,13]. This pathway was first identified for its role in segment polarity during *Drosophila* embryo development [14]. Since that discovery, Hh has been found to be a critical pathway in regulating cell differentiation and growth across model organisms. In humans, mutations in the Hh pathway have been linked to both developmental abnormalities and disease later in life, making it a relevant diagnostic and therapeutic target [15].

The Hh pathway starts with the Hedgehog (Hh) ligand binding to the transmembrane receptor Patched (Ptc). When unbound, Ptc inhibits Smoothed (Smo). The binding of Hh to Ptc stops the suppression of Smoothed, leading to downstream repression of proteins including Protein Kinase A (PKA) and the kinesin Costal-2 (Cos2) [16]. In the absence of Hh, PKA/Cos2 kinase complex phosphorylates Cubitus interruptus (Ci), which promotes proteolytic processing of Ci into a transcriptional repressor [17]. Hh inhibits Ci phosphorylation by PKA/Cos2 and the formation of Ci repressor form, allowing the accumulated full-length Ci to translocate into the nucleus and act as a transcriptional activator [18]. Ci has several known transcriptional targets including *Ptc*, which then serves as a negative feedback loop for the pathway [19].

Previously, we reported on *Ptc^{B.2.13}*, that was identified as a conditional regulator of overgrowth [8]. The *Ptc^{B.2.13}* mutation leads to non-autonomous overgrowth driven by the non-autonomous activity of Yorkie and pMad in cells that are adjacent to the *Ptc^{B.2.13}* clones. Complementing these findings was a companion

study utilizing the *GMR-Hid* mosaic screen conducted by the Bergmann lab [20].

Here, we add to the knowledge of the interplay between growth regulation, tissue development, and cell survival in the Hh pathway. We find that *Cos2* is also a Hh pathway conditional regulator of cell growth, dependent upon a block in the canonical apoptosis pathway. However, despite both *Ptc* and *Cos2* serving as negative regulators of the Hh signalling pathway, we find differences in the autonomous nature of the overgrowth: *Ptc* mutant clones drive a non-autonomous overgrowth, while *Cos2* mutant clones lead to both an autonomous and non-autonomous overgrowth. These findings provide insight into how disruptions to different points of the Hh signalling pathway lead to different consequences for growth and development.

Methods

Conditional genetic screen for regulators of cell growth and division

An EMS screen was conducted on chromosome 2R utilizing Flp/FRT system in the *Drosophila* eye. This screen utilized *FRT42D*, *Dark⁸²* as a starting chromosome to identify mutations that disrupted cell division and growth, dependent on the *Dark⁸²* block of apoptosis [8]. The *Dark⁸²* allele utilized has been shown to block developmental apoptosis when homozygous [21]. From the screen, 137 mutants were identified, and stable stocks were created. Selected growth mutants were mapped via complementation mapping to the Bloomington 2R Deficiency kit [22]. Previously, we mapped a novel allele of *Patched* (*Ptc^{B.2.13}*) [8]. From the same screen here, we report a novel allele of *Costal-2* (*Cos2^{F.1.4}*). The mutant stock *Cos2^{F.1.4}* failed to complement two previously characterized alleles of *Cos2*, *Cos2^{k16101}* and *Cos2^{H29}* [23,24].

To identify the specific molecular lesion causing the growth phenotypes in *Ptc* and *Cos2*, PCR primers were designed to the exons of each gene to identify the underlying molecular lesion. DNA was isolated utilizing Li/Cl, KAc from heterozygous *Ptc^{B.2.13}* and *Cos2^{F.1.4}* animals. Following successful PCR amplification, samples were sent for

Sanger sequencing to identify heterozygous point mutations in the chromatograms (Genewiz, New Jersey).

Genetics

In addition to the *Dark*⁸² allele [21], the following genotypes were used in these experiments *Ey-Flp; FRT42D* (BDSC), *Ey-Flp; FRT42D, ubi-GFP, Ey-Flp; FRT42D, M(2)* (BDSC), *UBX-Flp; FRT42D, ubi-GFP* (BDSC), *Cos2*^{H29} allele [23], *Cos2*^{K161010} (BDSC) [24], *Cos2*^{P50} [25], and *Ptc*^{S2} [26]. The 2R deficiency kit from the Bloomington *Drosophila* Stock Center was used for genetic mapping via complementation tests [22]. All crosses were conducted at 25°C.

Adult eye and wing visualization

Images were taken of the adult mosaic eyes at the same magnification (40x) under 70% ethanol to compare the size of eye and the ratio of mutant/wild-type tissue. In cases where the cross was set up to a stock containing the pigmented *Dark*⁸² allele, the 'Flp' stock contained an unpigmented *FRT42D* chromosome. When the *Dark*⁸² allele was not present, the 'Flp' stock utilized an *FRT42D* chromosome with pigmentation (*FRT42D, ubi-GFP*). Adult wings were mounted to slides in vegetable oil and imaged at the same magnification (70x) to allow comparison of size differences between genotypes. Quantification of adult wing size was done measuring pixels on Photoshop of at least 10 wings per genotype. For both wings and eyes, the images were taken on an AM Scope camera (AM scope 550 MA).

Immunohistochemistry

Imaginal eye and wing discs were dissected from wandering L3 larvae as previously described [8,27]. Briefly, imaginal discs were fixed in 4% paraformaldehyde and permeabilized in 0.3% PBST prior to staining with antibodies. Antibodies from Developmental Studies Hybridoma Bank: anti-Ptc (mouse, 1:40), anti-Elav (rat 1:800) and anti-Ci (rat, 1:100) were used to stain eye and wing discs. Other antibodies used were anti-phospho-Smad1/5 (pMad) (rabbit 1:100, Cell Signalling),

anti-DIAP1 (mouse, 1:50) [28], and anti-GFP (chicken, 1:100, Aves Labs). Imaginal eye and wing discs were visualized on a compound fluorescent microscope or confocal microscope using the Zen microscopy software (Zeiss microscopy).

Analysis of fluorescent images

Imaginal eye and wing disc size and autonomy were calculated using Photoshop to measure the number of pixels in each genotype. At least 10 imaginal discs were quantified for each genotype. Autonomy was determined by calculating the percentage of non-GFP (mutant) tissue divided by the whole tissue size using pixels in Photoshop. T-tests were used to analyse the differences in autonomy between *Ptc*^{B.2.13} and *Cos2*^{F.1.4} mosaic tissue, and p values were calculated to determine the significance. For these comparisons, a p value <0.05 was used for significance. To measure the levels of pMad expression across the clonal boundaries, fluorescent intensity was measured using the Zen microscopy line scan to measure signal intensity (Zeiss microscopy).

Results

Ptc and *Cos2* alleles were isolated from a conditional Flp/FRT eye screen and mapped to genes in the Hedgehog pathway

In the genetic background of blocked apoptosis, mutants that disrupted cell growth and cell division in the mosaic eye were isolated in an EMS Flp/FRT genetic screen [8]. Previously, *Ptc*^{B.2.13} was mapped as a novel allele of *Ptc* via complementation mapping, which resulted in a failure to complement the *Ptc*^{S2} allele [8,26].

We mapped the *F.1.4* mutant using homozygous lethality and complementation tests to the 2R Df kit [22]. A region of failure to complement was identified in the overlapping region between the deficiencies *Df(2R)ED1715* and *Df(2R)1673* from 2R:7,326,951.7,533,553. The *F.1.4* mutant was mated to individual alleles within this region and failed to complement two previously characterized *Cos2* alleles, *Cos2*^{K161010} and *Cos2*^{H29}, indicating that *Cos*^{F.1.4} is a novel allele of *Cos2* [23,24].

To further confirm the location of these mutations and to understand the molecular alterations, we conducted Sanger sequencing of both heterozygous *Ptc*^{B.2.13} and *Cos2*^{F.1.4} flies. For *Ptc*^{B.2.13} and *Cos2*^{F.1.4}, a double-peak in each chromatogram was observed resulting in missense mutations in an amino acid conserved between flies and humans. In *Ptc*^{B.2.13}, a T to A at 2R:8,660,339 was identified resulting in a Trp-173-Arg missense mutation (Supplemental Figure 1). In *Cos2*^{F.1.4}, a T to A at 2R:8,660,339 was identified, resulting in a Leu-951-Gln missense mutation (Supplemental Figure 1). The identified missense mutations along with the failure to complement data from established *Ptc* and *Cos* alleles establish *Ptc*^{B.2.13} and *Cos2*^{F.1.4} as mutant alleles of the Hh pathway.

***Ptc* and *Cos2* are conditional growth mutants necessary for eye development**

We previously reported on the non-autonomous overgrowth of the *Ptc*^{B.2.13}, *Dark*⁸² mosaic eyes as compared to the control *Dark*⁸² mosaic eyes (Figure 1a compared to 1b, mutant tissue is pigmented) [8]. Here, we add that *Cos2*^{F.1.4}, *Dark*⁸² also results in dramatically overgrown mosaic eye when compared to the control mosaic *Dark*⁸² (Figure 1a compared to 1c, mutant tissue pigmented). To visualize the ommatidial organization of the eye, we mated mutants to an *FRT42D* chromosome with GFP (*Ey-Flp; FRT42D, ubi-GFP*). Fluorescent apotome images show the *Dark*⁸² mosaic eye to have organized and patterned ommatidial structure in both the *Dark*⁸²/*Dark*⁸² clones (darker tissue) and adjacent wild-type clones (brighter GFP positive tissue) (Figure 1d). In contrast, both *Dark*⁸², *Ptc*^{B.2.13} and *Dark*⁸², *Cos2*^{F.1.4} have a disrupted ommatidial organization that can be visualized by the misalignment of ommatidia throughout the eye, the disruption of ommatidial organization can be seen in both mutant clones (darker tissue) and wild-type clones (lighter tissue) suggesting that Hh pathway disruption has both autonomous and non-autonomous effects on overall eye development (Figure 1e–f).

To investigate the degree to which the block in apoptosis contributes to the overgrowth phenotypes, we reintroduced the wild-type *Dark* allele

through recombination, allowing homozygous cells to again go through apoptosis in mosaic eyes. Without a block in apoptosis, both *Ptc*^{B.2.13} and *Cos2*^{F.1.4} mosaic eyes depict a partial rescue of overgrowth, indicating that both mutant overgrowth phenotypes are, at least in part, dependent upon a block in apoptosis (Figure 1g–h, mutant tissue unpigmented). Though the eyes size is reduced when apoptosis is reintroduced, eye organizational disruption remains and can be observed in both Hh mutants. Additionally, both *Ptc*^{B.2.13} or *Cos2*^{F.1.4} mosaic eyes had a reduction in visible unpigmented tissue (mutant tissue) as compared with *Dark*⁸², *Ptc*^{B.2.13} and *Dark*⁸², *Cos2*^{F.1.4}, which indicates that the majority (if not all) of the mutant cells may have been cleared by apoptosis upon the reintroduction of the wild-type *Dark* allele.

We next generated eyes entirely comprised mutant tissue by mating the *Ptc*^{B.2.13} and *Cos2*^{F.1.4} mutants to an FRT chromosome with a homozygous lethal mutation (*minute*). The *minute/minute* clones are eliminated via apoptosis, leaving behind a developing eye disc that is entirely mutant for either *Ptc*^{B.2.13}, *Dark*⁸² or *Cos2*^{F.1.4}, *Dark*⁸². In both cases, *Ptc*^{B.2.13}, *Dark*⁸² and *Cos2*^{F.1.4}, *Dark*⁸² mutants resulted in pupal lethality and a severe reduction in overall head size, highlighting the need for functional Hedgehog signalling in the developing eye and overall organismal survival (Figure 1i–j).

***Ptc* and *Cos2* mutations drive conditional overgrowth and pupal lethality in the mosaic wing**

To better understand the generalized nature of this conditional Hh-deregulated overgrowth, we analysed mosaic wing discs phenotypes utilizing the *UBX-Flp* driver. Previously, we found that *Ptc*^{B.2.13}, *Dark*⁸² mosaic wing led to a dramatic tissue overgrowth, resulting in pupal lethality due to wing size [8]. Here we find that similar to *Ptc*^{B.2.13}, *Dark*⁸² (Figure 2b), the *Cos2*^{F.1.4}, *Dark*⁸² mosaic wing discs result in substantial tissue overgrowth and complete pupal lethality (Figure 2a compared to 2c). While both the *Ptc*^{B.2.13}, *Dark*⁸² and *Cos2*^{F.1.4}, *Dark*⁸² mosaic wing discs were

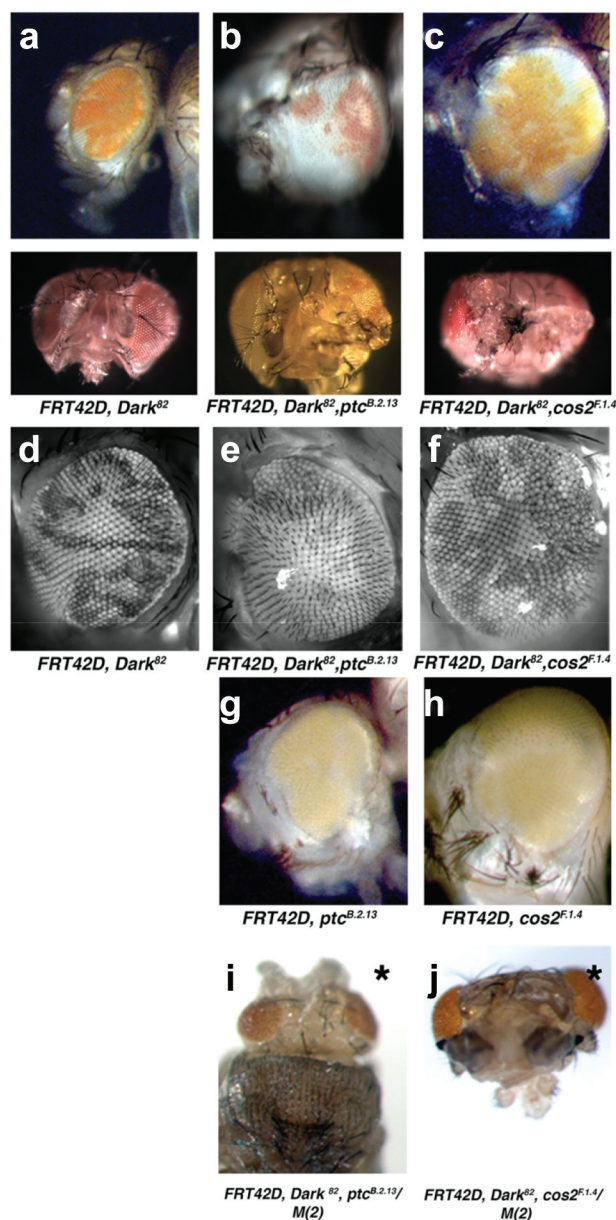


Figure 1. Alleles of *Patched* and *Costal-2* isolated from the same conditional Flp/FRT screen as negative regulators of cell growth and cell division in the eye. Mosaic adult eyes imaged via light microscopy by mating *Ey-Flp;FRT42D* to (a) control eye *FRT42D, Dark⁸²* (b) *FRT42D, ptc^{B.2.13}, Dark⁸²* (c) *FRT42D, Cos2^{F.1.4}, Dark⁸²* (mutant tissue pigmented via *mw+* in *Dark⁸²* allele). Fluorescent apotome images to visualize ommatidial organization by mating *Ey-Flp;FRT42D, ubi-GFP* to (d) control eye *FRT42D, Dark⁸²* (e) *FRT42D, ptc^{B.2.13}, Dark⁸²* (f) *FRT42D, Cos2^{F.1.4}, Dark⁸²* (mutant tissue, darker, fluorescent negative). Light microscope images without *Dark⁸²* allele through mating *Ey-Flp;FRT42D, ubi-GFP* to (g) *FRT42D, ptc^{B.2.13}* (h) *FRT42D, Cos2^{F.1.4}* (mutant tissue is non-pigmented). Light microscope images of eyes comprised entirely of mutant tissue by mating *Ey-Flp;FRT42D, M(2)* to (i) *FRT42D, ptc^{B.2.13}, Dark⁸²* (j) *FRT42D, Cos2^{F.1.4}, Dark⁸²* (mutant tissue is pigmented *mw+*). * denotes pupal lethality.

substantially larger than the *Dark⁸²* control disc, we noted that the overall size of the *Ptc^{B.2.13}, Dark⁸²* mosaic disc was consistently larger than the *Cos2^{F.1.4}, Dark⁸²* mosaic wing disc, though the difference was not statistically significant ($p = 0.06355497$) (Figure 2d). Despite there not

being a statistical difference in size, there was an observable biological difference between *Ptc^{B.2.13}* and *Cos2^{F.1.4}* mutants when the ability to undergo apoptosis was re-introduced by recombining the wild-type *Dark^{WT}* allele. The reintroduction of apoptosis (via *Dark⁺*) fully rescued the *Cos2^{F.1.4}*

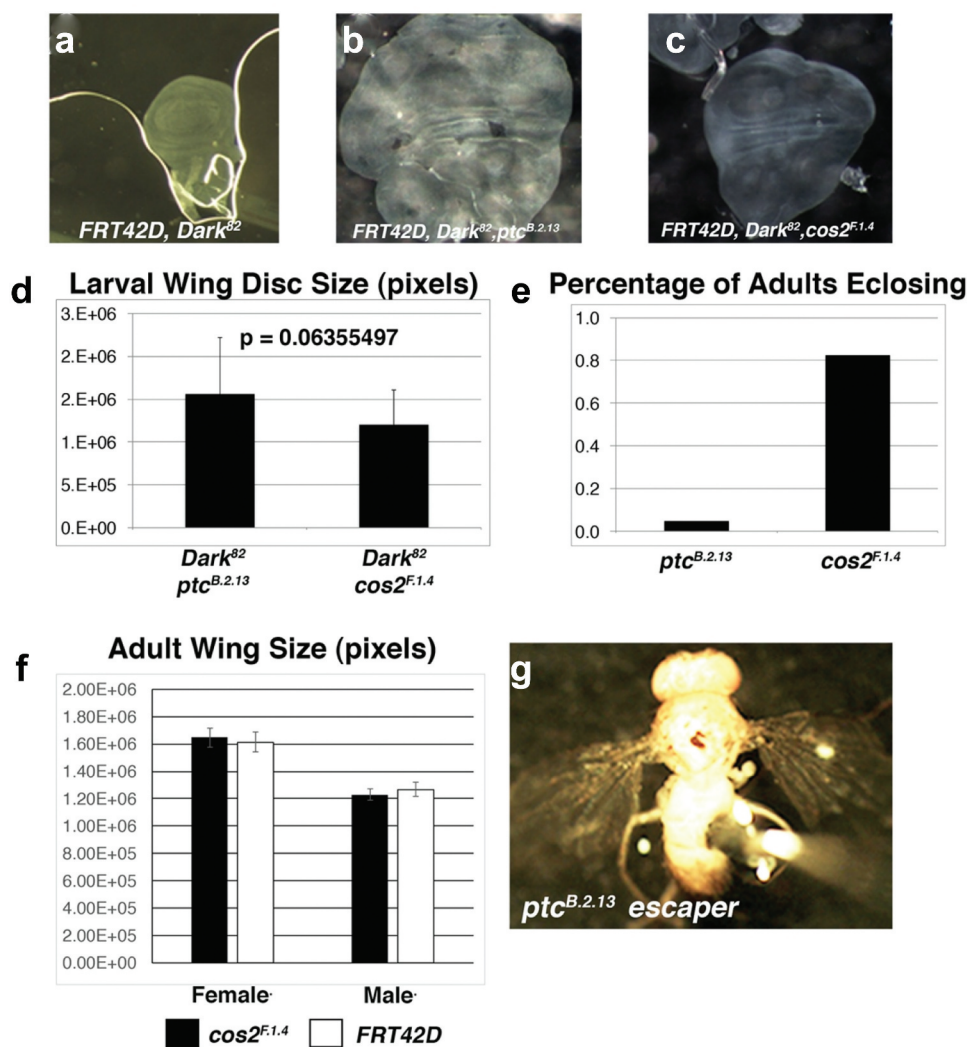


Figure 2. *Ptc^{B.2.13}* and *Cos2^{F.1.4}* exhibit conditional overgrowth phenotypes in the *Drosophila* wing that result in pupal lethality. Third instar imaginal wing discs were visualized by light microscopy for *UBX-Flp:FRT42D* mated to (a) control eye *FRT42D, Dark⁸²* (b) *FRT42D, ptc^{B.2.13}, Dark⁸²* (c) *FRT42D, Cos2^{F.1.4}, Dark⁸²*. Both *Ptc* and *Cos2* wing discs resulted in complete pupal lethality. Average size of third instar imaginal wing disc (in pixels) for (d) *FRT42D, ptc^{B.2.13}, Dark⁸²* and *FRT42D, Cos2^{F.1.4}, Dark⁸²* mosaic wing discs. Error bars represent standard deviation. Difference is not statistically significant. (e) Percentage of adults that eclosed without *Dark⁸²* allele for *FRT42D, ptc^{B.2.13}* and *FRT42D, Cos2^{F.1.4}*. (f) Comparison of adult wing size (in pixels) of control (*FRT42D*) and (*FRT42D, Cos2^{F.1.4}*) wings, 10 wings per genotype and sex. (g) Image of *FRT42D, ptc^{B.2.13}* escaper, depicting wings held out phenotype.

mosaic pupal lethality, while the majority of *Ptc^{B.2.13}* mosaic organisms still succumbed to pupal lethality (Figure 2e). Furthermore, the resulting *Cos2^{F.1.4}* mosaic wings were indistinguishable in size from control mosaic wings (Figure 2f). The rare *Ptc^{B.2.13}* escaper still had enlarged adults wing and depicted the ‘wings held out’ phenotype (Figure 2g). So while both *Ptc^{B.2.13}* and *Cos2^{F.1.4}* result in dramatic wing overgrowth, there are differences in the extent of tissue overgrowth based on which part of the Hh pathway is disrupted.

Patched and Costal-2 exhibit differences in the autonomy of overgrowth

While both *Ptc^{B.2.13}* and *Cos2^{F.1.4}* are conditional regulators of cell growth and tissue size, we observed differences in the ratio of mutant (pigmented) to wild-type (unpigmented) tissue (Figure 1(b,c)). The *Dark⁸², Ptc^{B.2.13}* mosaic eye is comprised of mostly wild-type tissue, suggesting a non-autonomous overgrowth (Figure 1(b,e) and [8]), while the *Dark⁸², Cos2^{F.1.4}* mosaic eye depicts more gross overgrowth (both autonomous and

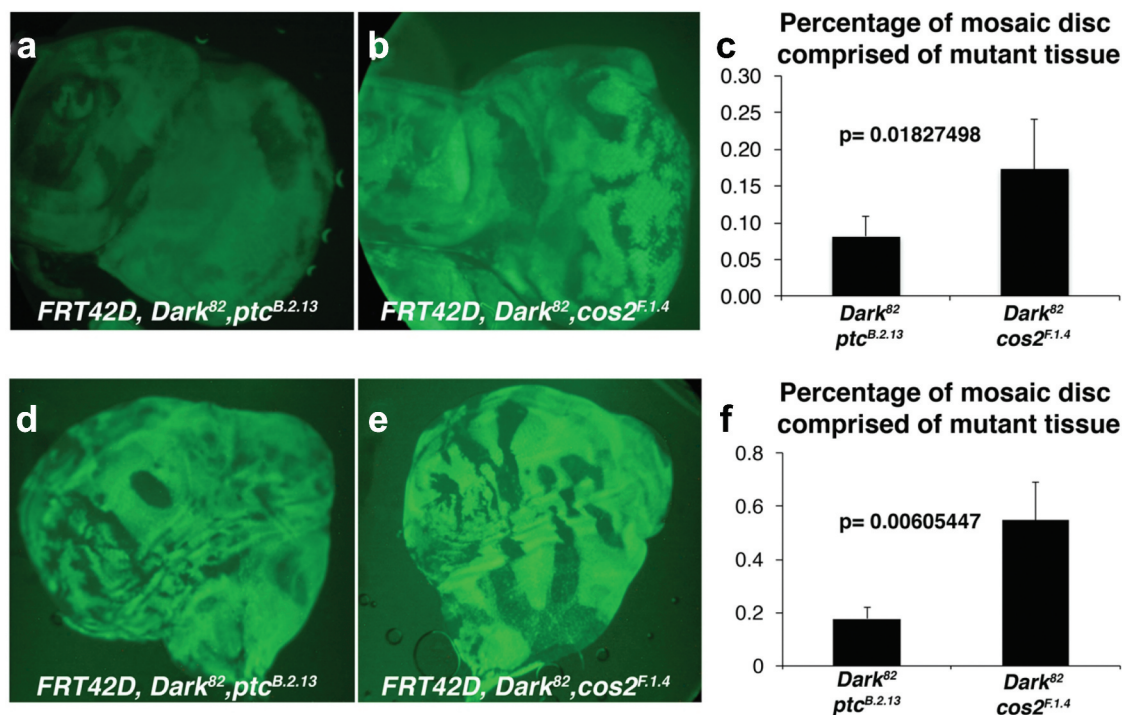


Figure 3. *Ptc^{B.2.13}* and *Cos2^{F.1.4}* exhibit distinct types of autonomous overgrowth in the eye and wing. Third instar imaginal eye discs were visualized by fluorescent microscopy for crosses of *Ey-Flp;FRT42D, ubi-GFP* mated to (a) *FRT42D, Ptc^{B.2.13}, Dark⁸²* (b) *FRT42D, Cos2^{F.1.4}, Dark⁸²* (homozygous mutant tissue is GFP negative). (c) Percentage of mosaic disc comprised mutant tissue for *FRT42D, Ptc^{B.2.13}, Dark⁸²* and *FRT42D, Cos2^{F.1.4}, Dark⁸²* measured by pixels. >10 imaginal discs quantified for each genotype. Error bars represent standard deviation and p value is from paired T-test. Third instar imaginal wing discs were visualized by light microscopy for crosses of *UBX-Flp;FRT42D, ubi-GFP* mated to (d) *FRT42D, Ptc^{B.2.13}, Dark⁸²* (e) *FRT42D, Cos2^{F.1.4}, Dark⁸²* (homozygous mutant tissue is GFP negative). Anterior portion of the wing disc oriented to the right. (f) Percentage of mosaic disc comprised mutant tissue for *FRT42D, Ptc^{B.2.13}, Dark⁸²* and *FRT42D, Cos2^{F.1.4}, Dark⁸²* measured by pixels. >10 imaginal discs quantified for each genotype. Error bars represent standard deviation and p value shown from paired T-test.

non-autonomous tissue overgrowth Figure (1 c,f)). To measure the extent of this difference, we utilized imaginal eye and wing discs to determine the percentage each disc is comprised of homozygous mutant tissue in *Ptc^{B.2.13}* and *Cos2^{F.1.4}* mutants. Using imaginal discs allowed for quantification of 2-D tissue instead of 3-D eye ratios. In these imaginal discs, we observe a statistically significant difference ($p = 0.01827498$) in which the *Dark⁸², Ptc^{B.2.13}* eye discs are comprised of (8.1%) mutant tissue (non-GFP positive), while the *Dark⁸², Cos2^{F.1.4}* eye discs are comprised of (17.2%) mutant tissue (non-GFP positive) (Figure 3(a-c)). This difference in autonomous overgrowth exists between mutants despite both genotypes resulting in premature differentiation (and mitotic arrest) in the imaginal eye discs (observed by ectopic *Elav* expression before the morphogenetic furrow in

both *Ptc^{B.2.13}* and *Cos2^{F.1.4}* mosaic eye discs, (Supplemental Figure 2). Similarly, in the wing disc, we find that 12.6% of *Dark⁸², Ptc^{B.2.13}* imaginal wing discs are comprised of mutant tissue, while 25.9% of *Dark⁸², Cos2^{F.1.4}* imaginal wing discs are comprised of mutant tissue, $p = 0.00605447$ (Figure 3(d-f)). As a comparison, we have previously reported the *Dark⁸²* mosaic wing disc to be ~38% *Dark⁸²/Dark⁸²* mutant cells. The difference in tissue autonomy of *Ptc* and *Cos2* in the eye and wing overgrowth autonomy suggest that these are pathway disruption differences and not a phenomenon of tissue-specific developmental signalling. To understand how mutations in the same pathway could lead to different varieties of tissue overgrowth, we utilized imaginal disc staining to observe molecular alterations that accompany these mutations.

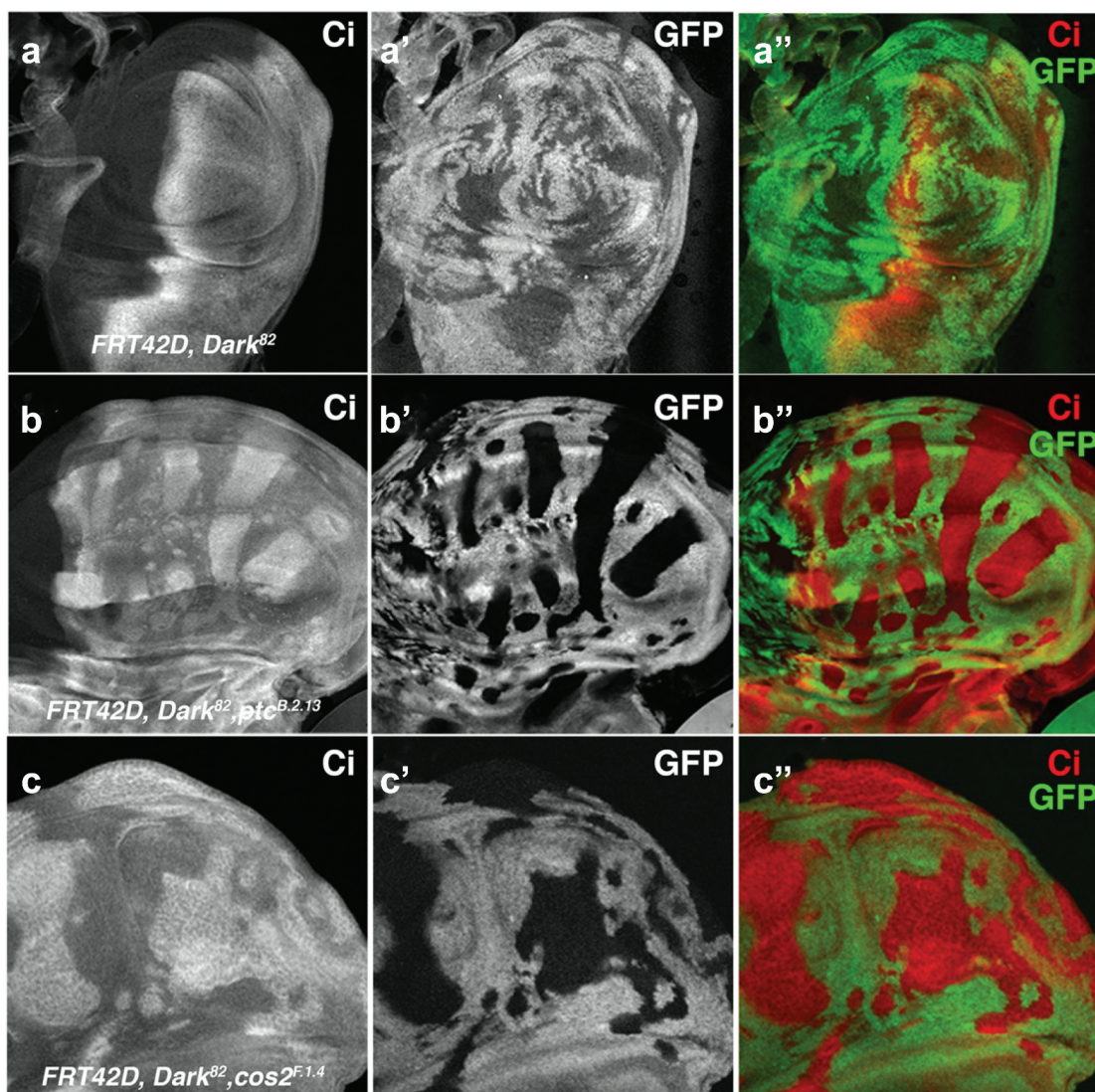


Figure 4. *Ptc*^{B.2.13} and *Cos2*^{F.1.4} autonomously upregulated Ci within mutant clones in the anterior compartment of imaginal wing discs. Ci levels visualized in third instar imaginal wing discs through staining and fluorescent microscopy for crosses of *UBX-Flp;FRT42D, ubi-GFP* mated to (a) control *FRT42D, Dark*⁸² (b) *FRT42D, Ptc*^{B.2.13}, *Dark*⁸² (c) *FRT42D, Cos2*^{F.1.4}, *Dark*⁸² (mutant tissue is GFP negative). Anterior portion of wing discs are oriented to the right.

Additional alleles of both *Ptc* and *Cos2* were studied to determine if the difference in overgrowth autonomy observed in *Ptc*^{B.2.13} and *Cos2*^{F.1.4} is consistent across independently generated alleles. We utilized two previously characterized alleles *Ptc*^{S2} and *Cos2*^{P50} [25,26]. Both alleles were recombined to include the *Dark*⁸² allele and adult mosaic eyes were visualized as Z-stacks. We find that the difference in overgrowth autonomy is consistent across alleles. *Dark*⁸², *Ptc*^{S2} mosaic eyes demonstrate a severely overgrown adult eye that is comprised mostly of wild-type tissue (non-autonomous overgrowth). This finding is similar

to our *Dark*⁸², *Ptc*^{B.2.13} mosaic eye (compare Figure 1e with supplemental Figure 3b). Additionally, we find that *Dark*⁸², *Cos2*^{P50} generates a severely overgrown and disorganized adult eye comprised of fairly equal ratios of homozygous mutant and wild-type tissue similar to *Dark*⁸², *Cos2*^{F.1.4} (compare Figure with supplemental Figure 3c). The consistent difference observed in *Cos2* and *Ptc* conditional overgrowth across independently generated alleles suggests that this difference is not specific to the *Ptc*^{B.2.13} and *Cos2*^{F.1.4} alleles but generalizable to mutations in these genes.

***Ptc* and *Cos2* autonomously deregulate Hedgehog pathway signalling**

Both *Ptc* and *Cos2* are upstream negative regulators of the canonical Hedgehog signalling pathway and function to sequester the transcription factor Cubitus interruptus (Ci) in the cytoplasm [29]. Previously, we established that *Ptc*^{B.2.13} mutant clones result in an autonomous upregulation of Dpp, Patched, and Ci (Figure 4b, [8]). *Cos2* mutations have also been shown to autonomously upregulate downstream Hh targets [23,25,30]. Here, we support these findings through the observation of an upregulation of cleaved Ci in *Dark*⁸², *Ptc*^{B.2.13} and *Dark*⁸², *Cos2*^{F.1.4} imaginal wing disc clones (Figure 3(b–c)). Conversely, *Dark*⁸² mosaic wings demonstrate a wild-type expression pattern of Ci, suggesting that the Ci overexpression is not resultant from a block in apoptosis (Figure 3a). The deregulation of Ci in *Ptc* and *Cos2* mutants occurs exclusively in clones on the anterior side of the wing disc correspondent with the expression domain of Ci (all wing discs are oriented with anterior to the right). *Dark*⁸², *Cos2*^{F.1.4} also phenocopies the *Dark*⁸², *Ptc*^{B.2.13} autonomous increase of Patched expression in the anterior domain of the wing disc (*Ptc* is also a Ci target gene) (Supplemental Figure 4). Overall, this suggests that mutations in *Ptc* or *Cos2* disrupt the Hh pathway and lead to an autonomous increase of Hh signalling.

***Ptc* and *Cos2* mutant clones result in a non-autonomous upregulation of DIAP1**

Previously, our lab and others have established a link between Hh deregulation and non-autonomous DIAP1 upregulation in both *Ptc* and *Cos2* mosaic tissue [8,23,25]. To ensure this non-autonomous upregulation of DIAP1 is consistent across *Cos2* alleles, we measured the levels of DIAP1 expression in mosaic imaginal wing discs for *Cos2*^{F.1.4}. As conveyed previously, *Dark*⁸², *Ptc*^{B.2.13} leads to the non-autonomous upregulation of DIAP1 (Figure 5a), which can be visualized as the halo of DIAP1 expression just outside of the *Ptc*^{B.2.13} clonal borders. The *Dark*⁸², *Cos2*^{F.1.4} mutant also leads to the non-autonomous increase in DIAP1 expression (Figure 5b) visualized as

halos of DIAP1 upregulation immediately outside the *Cos2*^{F.1.4} clones. To more easily visualize the non-autonomous nature of the DIAP1 overexpression, we utilized Ci to mark the mutant clones, which provides an easier observation of expression at the clonal boundaries. Further, this upregulation of DIAP1 is confined to the anterior compartment suggesting it is dependent on the Ci overexpression autonomously to facilitate the non-autonomous DIAP1 upregulation (Figure 5).

***Ptc* and *Cos2* mutations have different patterns of deregulated pMad**

Previously, we found that the non-autonomous increase in DIAP1 and non-autonomous tissue proliferation of the *Dark*⁸², *Ptc*^{B.2.13} mutants were shown to be dependent on the concurrent non-autonomous up regulation of pMad and the interaction of pMad and Yorkie to drive non-autonomous survival and proliferation [8]. Here, we investigated if *Cos2*^{F.1.4} mutant clones also deregulate pMad in a similar manner. The non-autonomous activation of pMad in *Dark*⁸², *Ptc*^{B.2.13} mosaic wing discs, is visualized by the demonstrable increase in pMad expression just outside of the mutant clone (mutant clones again marked by Ci expression to visualize pMad expression at the clonal boundaries) (Figure 6a–a’). This non-autonomous increase is also seen via line scan, where the peaks of pMad expression are just outside of the mutant clonal boundaries and dissipate further away from the mutant clone (Figure 6b, clones marked by arrows).

In *Dark*⁸², *Cos2*^{F.1.4} clones we also see a deregulation and overexpression of pMad expression. However, in contrast to the predominantly non-autonomous mis-expression seen in the *Ptc*^{B.2.13} clones, in *Cos2*^{F.1.4} the upregulation of pMad is more balanced between autonomous (within the clone) and non-autonomous (adjacent to the clone) mis-expression (Figure 6 (c’–c’)), mutant clones marked by Ci to visualize boundary expression). A line scan was used to visualize the pMad expression intensity. The high levels of pMad expression came from within the mutant clone and then remained high outside the clonal boundary (Figure 6d, clonal boundaries arrows). This indicates that while both *Ptc* and *Cos2* mutant

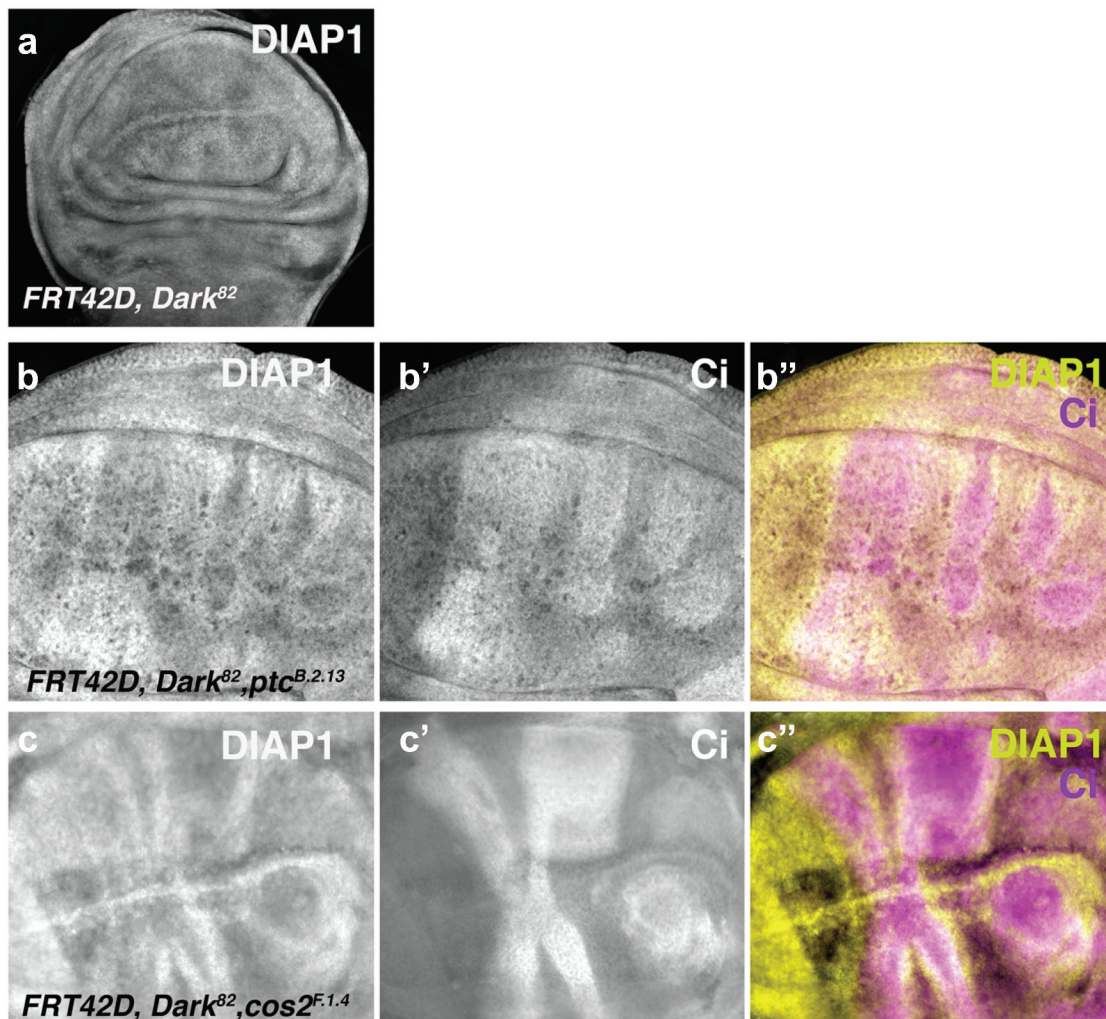


Figure 5. *Ptc^{B.2.13}* and *Cos2^{F.1.4}* non-autonomously upregulated DIAP1 just outside of mutant clone boundaries in the anterior compartment of imaginal wing discs. DIAP1 levels visualized in third instar imaginal wing discs through staining and fluorescent microscopy for crosses of *UBX-Flp;FRT42D, ubi-GFP;FRT42D, ubi-GFP* mated to (a) *FRT42D, Dark⁸²* mosaic stained with DIAP1. (b-b'') *FRT42D, ptc^{B.2.13}, Dark⁸²* stained with DIAP1 and Ci (to mark homozygous mutant clones) (c-c'') *FRT42D, Cos2^{F.1.4}, Dark⁸²* stained with DIAP1 and Ci (to mark homozygous mutant clones). Anterior portion of wing discs are oriented to the right.

tissue lead to a non-autonomous increase of pMad, only *Cos2* has an autonomous upregulation of pMad expression. The regions in which pMad overexpression is observed correlate to the nature of tissue overgrowth, non-autonomous, for *Ptc^{B.2.13}* and both autonomous and non-autonomous for *Cos2^{F.1.4}*. The pattern of pMad expression was consistent across numerous clones for each mutant type and the patterns of *Ptc* and *Cos2* deregulation of pMad expression are diagrammed in Supplemental Figure 5.

Discussion

Overview

We designed a genetic screen to identify negative regulators of cell growth and cell division that were conditional for a block in apoptosis. From this screen, we isolated and mapped a novel allele of *Cos2*, *Cos2^{F.1.4}*, as a conditional growth regulator from an EMS Flp/FRT mosaic eye screen. This finding builds upon previous data where we identified another member of the hedgehog signalling pathway, *Ptc^{B.2.13}*, in the same screen, providing confirmation that disruption in the hedgehog pathway can lead to conditional tissue overgrowth in *Drosophila* [8]. While both *Ptc* and *Cos2*

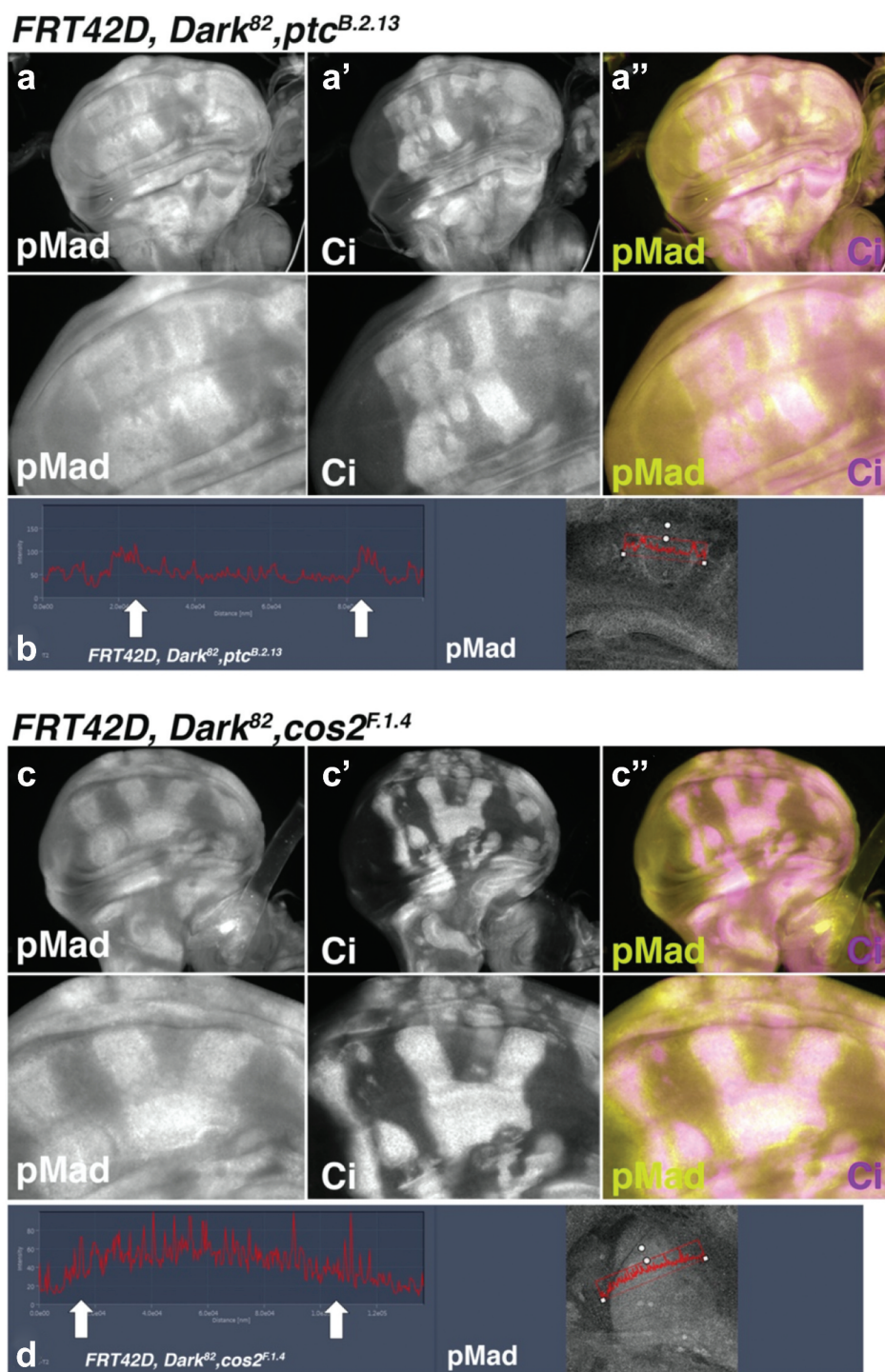


Figure 6. *Ptc^{B.2.13}* and *Cos2^{F.1.4}* differentially upregulated pMad inside mutant clones. pMad levels visualized in third instar imaginal wing discs through staining and fluorescent microscopy for crosses of *UBX-Flp;FRT42D, ubi-GFP* mated to (a-a'') *FRT42D, Ptc^{B.2.13}, Dark⁸²* (mutant tissue are marked by Ci upregulated tissue) (b) quantification of pMad1/5 levels across the mutant clonal boundaries in *Ptc^{B.2.13}* mutant clones. Arrows denote clonal boundaries. (c-c'') *FRT42D, Cos2^{F.1.4}, Dark⁸²* (mutant tissue are marked by Ci upregulated tissue) (d) quantification of pMad levels across the mutant clonal boundaries in *Ptc^{B.2.13}* mutant clones. Arrows denote clonal boundaries. Anterior portion of wing discs are oriented to the right.

mutants result in dramatic eye and wing overgrowth due to the autonomous disruption of the Hh pathway, we observed that the nature of the

overgrowth differs between *Ptc* and *Cos2* mutants. *Ptc* mosaic tissue displays a distinct non-autonomous overgrowth, whereas *Cos2* mosaic

tissue results in both autonomous and non-autonomous overgrowth. These differences were consistent in both the eye and wing imaginal discs. Our data indicate that this difference may be due to the differential pattern of pMad deregulation. The upregulation of pMad has previously been demonstrated to drive tissue overgrowth [8,31], and the pattern of pMad deregulation in *Ptc* and *Cos2* mosaic tissue directly matches the patterns of overgrowth.

While it remains a possibility that the differences may result from the specific nature of the mutation (null vs hypomorph etc.), we contend that these differences are based on the nature of the consequences of the mutated gene based on several pieces of data. 1. The non-autonomous difference between *Ptc*^{B.2.13}, *Dark*⁸² and *Cos2*^{F.1.4}, *Dark*⁸² is consistent across different types of tissue (eye and wing). 2. We find common disruption of the Hh pathway (through autonomous Ci and Ptc staining) and common non-autonomous survival (via DIAP1). 3. Both *Ptc* and *Cos2* alleles were identified in independent screens looking for mutations that impacted cell survival and cell growth.

Association of cell survival and Hedgehog signalling

Our results suggest that a functional Hh signalling pathway is necessary for cell survival in imaginal disc development. Mutations to the *Ptc* and *Cos2* members of the hedgehog pathway led to cell death. When apoptosis was blocked, *Ptc* and *Cos2* mutants depicted dramatic overgrowth, which was rescued in both the eye and wing when the wild-type *Dark* allele was reintroduced, thus reinstating cell death.

This is further supported by the findings of the Bergman lab that identified multiple members of the Hh pathway in the *GMR-Hid Flp/FRT* screen [20,23,25]. This study also observed an autonomous increase in cell death when the Hh pathway is disrupted. The finding that this cell death is accompanied by a concurrent non-autonomous survival signal may be due to the compensatory proliferation resulting from the loss of Hh-dependent cell death [32]. This

concurrent non-autonomous DIAP1 and proliferation increase could be a mechanism of tissue regeneration from which dying cells signal to their neighbours to proliferate. In our scenario, we have removed the ability of the Hh deficient cells to die through the canonical apoptotic pathway, therefore creating a constitutive non-autonomous survival and growth signalling leading to eye and wing overgrowth.

***Ptc* and *Cos2* exhibit different patterns of pMad deregulation**

Both *Ptc* and *Cos2* mutations lead to an autonomous increase in hedgehog signalling (including Ci, and Ptc); however, there may be a difference in which type of cells can interpret the increased Hh target Dpp. Given that Dpp is a morphogen, both autonomous and non-autonomous cells would receive the Dpp signal via the receptors Thick Veins and Punt [33]. However, as we previously demonstrated, the *Ptc*^{B.2.13} mutant clones also autonomously upregulated the inhibitory smad, Daughters Against Decapentaplegic (Dad) [8,34]. We hypothesize that a lack of Dad upregulation in the *Cos2*^{F.1.4} mutant clones would result in an autonomous increase proliferation due to the Dpp mediated pMad activation (as seen in Figure 6). Alternatively, it is possible that a differential downregulation of Tkv downstream of the Hh signalling could lead to the differential activation of pMad between *Ptc* and *Cos2* mutant clones [35]. In either scenario, the difference in autonomous pMad upregulation between *Ptc* and *Cos2* mosaic tissue highlights the importance of understanding how disrupting different points of conserved pathways impacts tissue patterning and growth.

Potential implications for understanding Hh disrupted human tumours

A detailed understanding of the precise genetic mechanisms and pathways leading to deregulated growth in Hh mutations will be important in developing diagnostic and treatment tools to address Hh deregulated tumours in humans. Hedgehog pathway mutations are associated with various types of human cancers, including medulloblastoma; basal cell carcinoma; glioma; and breast, colorectal,

pancreatic, and prostate cancer [16,36]. The loss of *Ptc* also increases the occurrence of these types of tumours in mice, providing additional models for study [37]. There is evidence of both *Ptc* and *Kif7* (the human homolog of *Cos2*) being down-regulated in different human cancers, including basal cell carcinoma and ovarian cancer [38]. Fully understanding the phenotypic differences that arise from disruptions at different points in the Hh pathway may ultimately help with personalized medicine and treatment decisions for patients with Hh-deregulated tumours.

Acknowledgments

We thank A. Bergmann, T. Cook, and K. Moberg for *Drosophila* stocks and reagents. We thank T. Cook and E. Kagey for helpful comments on earlier drafts of this manuscript. Antibodies were obtained from the Developmental Studies Hybridoma Bank, created by the NICHD of the NIH and maintained at The University of Iowa, Department of Biology, Iowa City, IA 52242. Stocks obtained from the Bloomington *Drosophila* Stock Center (NIH P40OD018537) were used in this study.

Disclosure statement

No potential conflict of interest was reported by the author(s).

Funding

This work was supported by the National Science Foundation (2021146 to KLB and JDK) and the National Institutes of Health BUILD initiative ReBUILDetroit (UL1GM118982, TL4GM118983, and RL5GM118981 to JDK and SJN); National Institute of General Medical Sciences (GM103440 to RLT and KLB).

Data availability

The authors confirm that the data supporting the findings of this study are available within the article [and/or] its supplementary materials.

ORCID

Richard L. Tillett  <http://orcid.org/0000-0002-6671-8627>
 Kayla L. Bieser  <http://orcid.org/0000-0001-5981-2650>
 Jacob D. Kagey  <http://orcid.org/0000-0002-6994-1795>

References

- [1] St Johnston D. The art and design of genetic screens: *Drosophila melanogaster*. *Nat Rev Genet*. 2002;3:176–188.
- [2] Hariharan IK, Bilder D. Regulation of imaginal disc growth by tumor-suppressor genes in *Drosophila*. *Annu Rev Genet*. 2006;40:335–361.
- [3] Harvey KF, Pflieger CM, Hariharan IK. The *Drosophila* Mst ortholog, hippo, restricts growth and cell proliferation and promotes apoptosis. *Cell*. 2003;114:457–467.
- [4] Moberg KH, Bell DW, Wahrer DC, et al. Archipelago regulates Cyclin E levels in *Drosophila* and is mutated in human cancer cell lines. *Nature*. 2001;413:311–316.
- [5] Wu S, Huang J, Dong J, et al. hippo encodes a Ste-20 family protein kinase that restricts cell proliferation and promotes apoptosis in conjunction with salvador and warts. *Cell*. 2003;114:445–456.
- [6] Golic KG, Lindquist S. The FLP recombinase of yeast catalyzes site-specific recombination in the *Drosophila* genome. *Cell*. 1989;59:499–509.
- [7] Hanahan D, Weinberg RA. The hallmarks of cancer. *Cell*. 2000;100:57–70.
- [8] Kagey JD, Brown JA, Moberg KH. Regulation of Yorkie activity in *Drosophila* imaginal discs by the Hedgehog receptor gene patched. *Mech Dev*. 2012;129:339–349.
- [9] Brumby AM, Richardson HE. Scribble mutants cooperate with oncogenic Ras or Notch to cause neoplastic overgrowth in *Drosophila*. *EMBO J*. 2003;22:5769–5779.
- [10] Bieser K, Sanford J, Saville K, et al. Genetic mapping of *shn(E.3.2)* in *Drosophila melanogaster*. *MicroPubl Biol*. 2019;2019. doi:10.17912/micropub.biology.000118.
- [11] Cosenza A, Kagey JD. The mapping and characterization of Cruella (Cru), a Novel Allele of capping protein α (Cpa), identified from a conditional screen for negative regulators of cell growth and cell division. *Adv Biosci Biotechnol*. 2016;7:373–380.
- [12] Bellusci S, Furuta Y, Rush MG, et al. Involvement of Sonic hedgehog (Shh) in mouse embryonic lung growth and morphogenesis. *Development*. 1997;124:53–63.
- [13] Goodrich LV, Johnson RL, Milenkovic L, et al. Conservation of the hedgehog/patched signaling pathway from flies to mice: induction of a mouse patched gene by Hedgehog. *Genes Dev*. 1996;10:301–312.
- [14] Nusslein-Volhard C, Wieschaus E. Mutations affecting segment number and polarity in *Drosophila*. *Nature*. 1980;287:795–801.
- [15] Hahn H, Wicking C, Zaphiropoulos PG, et al. Mutations of the human homolog of *Drosophila* patched in the nevoid basal cell carcinoma syndrome. *Cell*. 1996;85:841–851.
- [16] Jiang J, Hui CC. Hedgehog signaling in development and cancer. *Dev Cell*. 2008;15:801–812.

- [17] Zhang W, Zhao Y, Tong C, et al. Hedgehog-regulated Costal2-kinase complexes control phosphorylation and proteolytic processing of Cubitus interruptus. *Dev Cell*. 2005;8:267–278.
- [18] Wang G, Amanai K, Wang B, et al. Interactions with Costal2 and suppressor of fused regulate nuclear translocation and activity of cubitus interruptus. *Genes Dev*. 2000;14:2893–2905.
- [19] Xiong Y, Liu C, Zhao Y. Decoding Ci: from partial degradation to inhibition. *Dev Growth Differ*. 2015;57:98–108.
- [20] Fan Y, Bergmann A. Apoptosis-induced compensatory proliferation. The cell is dead. Long live the cell! *Trends Cell Biol*. 2008;18:467–473.
- [21] Akdemir F, Farkas R, Chen P, et al. Autophagy occurs upstream or parallel to the apoptosome during histolytic cell death. *Development*. 2006;133:1457–1465.
- [22] Cook RK, Christensen SJ, Deal JA, et al. The generation of chromosomal deletions to provide extensive coverage and subdivision of the *Drosophila melanogaster* genome. *Genome Biol*. 2012;13:R21.
- [23] Christiansen AE, Ding T, Fan Y, et al. Non-cell autonomous control of apoptosis by ligand-independent Hedgehog signaling in *Drosophila*. *Cell Death Differ*. 2013;20:302–311.
- [24] Roch F, Serras F, Cifuentes FJ, et al. Screening of larval/pupal P-element induced lethals on the second chromosome in *Drosophila melanogaster*: clonal analysis and morphology of imaginal discs. *Mol Gen Genet*. 1998;257:103–112.
- [25] Christiansen AE, Ding T, Bergmann A. Ligand-independent activation of the Hedgehog pathway displays non-cell autonomous proliferation during eye development in *Drosophila*. *Mech Dev*. 2012;129:98–108.
- [26] Ingham PW, Taylor AM, Nakano Y. Role of the *Drosophila* patched gene in positional signalling. *Nature*. 1991;353:184–187.
- [27] Pellock BJ, Buff E, White K, et al. The *Drosophila* tumor suppressors expanded and Merlin differentially regulate cell cycle exit, apoptosis, and wingless signaling. *Dev Biol*. 2007;304:102–115.
- [28] Yoo SJ, Huh JR, Muro I, et al. Hid, Rpr and Grim negatively regulate DIAP1 levels through distinct mechanisms. *Nat Cell Biol*. 2002;4:416–424.
- [29] Aza-Blanc P, Ramirez-Weber FA, Laget MP, et al. Proteolysis that is inhibited by hedgehog targets Cubitus interruptus protein to the nucleus and converts it to a repressor. *Cell*. 1997;89:1043–1053.
- [30] Zadorozny EV, Little JC, Kalderon D. Contributions of Costal 2-Fused interactions to Hedgehog signaling in *Drosophila*. *Development*. 2015;142:931–942.
- [31] Oh H, Irvine KD. Cooperative regulation of growth by Yorkie and Mad through bantam. *Dev Cell*. 2011;20:109–122.
- [32] Worley MI, Setiawan L, Hariharan IK. Regeneration and transdetermination in *Drosophila* imaginal discs. *Annu Rev Genet*. 2012;46:289–310.
- [33] Hamaratoglu F, Affolter M, Pyrowolakis G. Dpp/BMP signaling in flies: from molecules to biology. *Semin Cell Dev Biol*. 2014;32:128–136.
- [34] Goldstein JA, Kelly SM, LoPresti PP, et al. SMAD signaling drives heart and muscle dysfunction in a *Drosophila* model of muscular dystrophy. *Hum Mol Genet*. 2011;20:894–904.
- [35] Tanimoto H, Itoh S, ten Dijke P, et al. Hedgehog creates a gradient of DPP activity in *Drosophila* wing imaginal discs. *Mol Cell*. 2000;5:59–71.
- [36] Skoda AM, Simovic D, Karin V, et al. The role of the Hedgehog signaling pathway in cancer: a comprehensive review. *Bosn J Basic Med Sci*. 2018;18:8–20.
- [37] Wu X, Northcott PA, Croul S, et al. Mouse models of medulloblastoma. *Chin J Cancer*. 2011;30:442–449.
- [38] Yao Y, Liu L, He W, et al. Low expression of KIF7 indicates poor prognosis in epithelial ovarian cancer. *Cancer Biomark*. 2019;26:481–489.